Applied Catalysis B: Environmental 242 (2019) 140–149

Contents lists available at ScienceDirect

Applied Catalysis B: Environmental

journal homepage: www.elsevier.com/locate/apcatb

Synergy between Ag nanoparticles and yttria-stabilized zirconia for soot oxidation

A. Serve[a], A. Boreave[a], B. Cartoixa[b], K. Pajot[c], P. Vernoux[a,*]

[a] Univ. Lyon, Université Claude Bernard Lyon 1, CNRS-IRCELYON-UMR 5256, 2 Avenue A. Einstein, 69626 Villeurbanne, France
[b] CTI, Céramiques Techniques Industrielles, 382 Avenue du Moulinas, 30340 Salindres, France
[c] Groupe PSA, Centre technique de Vélizy, Route de Gisy 78943 Vélizy-Villacoublay, France

ARTICLE INFO

Keywords:
Yttria-stabilized zirconia
Ag
Soot combustion
Diesel particulate filter
Isotopic oxygen exchange

ABSTRACT

This study investigates a potential synergy between Ag nanoparticles and Yttria-Stabilized Zirconia (YSZ), an oxygen ionically conducting support, for developing an efficient and stable catalyst for Diesel Particulate Filter regeneration only with oxygen. The catalytic performances as well as the mechanism for soot combustion were thoroughly analyzed through Temperature-Programmed Oxidation and isotopic experiments. We found that Ag/YSZ catalysts reach the highest activity for low contents of Ag, i.e. 2 wt%. Isotopic experiments were carefully performed to prove that active oxygen species originate from YSZ lattice. Silver was shown to promote soot oxidation activity by activating the dissociative adsorption of oxygen that can replenish the YSZ support.

1. Introduction

Since the use of a Diesel particle Filter (DPF) became widespread for Diesel passenger cars from 2009 (Euro 5 standard), various technologies have been investigated to improve the issue of DPF regeneration. As soot is collected and trapped in the DPF, a soot "cake" is formed and back-pressure occurs in the exhaust which can lead to engine failure if not tended to. When the back-pressure reaches a certain value, a post-injection of fuel is triggered. Organic compounds leaving the combustion chamber are oxidized by the Diesel oxidation Catalyst (DOC) situated upstream of the DPF. The reaction produces an exotherm, which increases the exhaust temperature at the DPF inlet and allows the thermal oxidation of the soot with oxygen from around 650 °C. These post-injections provoke fuel overconsumptions, which is not suitable for the objective of CO_2 emission reduction. Among the solutions which have emerged to limit the fuel post-injections, we can cite the Fuel-Borne strategy [1,2]. It implies the use of a catalyst precursor (cerium or iron oxide) introduced in the fuel, and then injected in the combustion chamber. Such method allows intimate contact between the soot and the catalyst, a parameter which is known to be essential for activity [2]. Oxidation is conducted through oxygen contained in ceria [3,4] and DPF regeneration can be achieved from around 550 °C instead of 650–700 °C without any catalysts. This strategy is now successfully implemented, but has two drawbacks, such as the necessity for a separate tank containing the catalyst precursor positioned near the diesel tank, which needs to be filled on a regular basis, and the deposit of ash in the DPF channels, as the catalyst is not burnt. Another way to regenerate DPF is the Continuously Regenerating Trap (CRT) strategy [2,5,6], where the soot is oxidized by NO_2 produced through a Pt supported catalyst. NO produced in the engine is oxidized to NO_2, which then directly reacts with the soot along the reactions (1) and (2):

$$2\ NO_{2(g)} + C_{(s)} \rightarrow 2\ NO_{(g)} + CO_{2(g)} \quad (1)$$

$$NO_{2(g)} + C_{(s)} \rightarrow NO_{(g)} + CO_{(g)} \quad (2)$$

In contrast to the soot oxidation with oxygen, the kinetics of these reactions is not limited by the soot/catalyst interface. However, the last Euro 6 standards have lowered the allowed NO_x emission. As a consequence, a DeNOx catalytic after-treatment has to be implemented in the exhaust to reduce NO_x emissions. These DeNOx systems are temperature-dependent; for instance, the urea-SCR (Selective Catalytic Reduction) strategy is more effective for temperatures higher than 180 °C [7,8]. This is a major issue for a DeNOx situated downstream of the DPF, far away from the engine, where the temperature could be quite low. As NOx abatement downstream of the DPF remains an issue, it is more efficient to place the DeNOx system upstream which means only oxygen remains suitable as an oxidant for soot combustion.

The catalyzed DPF strategy fits these conditions where NO_x is converted upstream: a soot oxidation catalyst is coated onto the inlet channels of the DPF. During soot collection, a fraction of the particles comes into contact with the catalyst and can be oxidized at lower

* Corresponding author.
E-mail address: philippe.vernoux@ircelyon.univ-lyon1.fr (P. Vernoux).

https://doi.org/10.1016/j.apcatb.2018.09.069
Received 6 April 2018; Received in revised form 10 September 2018; Accepted 19 September 2018
Available online 20 September 2018

temperatures. The produced exotherm allows the oxidation of the rest of the soot which is distant from the catalyst. In contrast to the CRT strategy where NO_x is used, the oxidation reaction runs with oxygen, either provided by the catalyst lattice or by the gas phase.

Soot oxidation catalysts have been widely studied in the literature; ceria-based catalysts [9–14] along with perovskites [15–22] display high activities, mostly related to their ability to produce highly active peroxide and superoxide oxygen species. Ceria is known to be able to change the valence state of Ce atoms from Ce^{4+} to Ce^{3+}, thus liberating an ionic oxygen species from its surface [11–13,23], while perovskites display numerous oxygen vacancies, allowing oxygen species to migrate from the lattice to the interface between the soot and the catalyst [14,17,19–21,24].

Recently, our group reported that YSZ (Yttria Stabilized Zirconia) displayed remarkable properties toward soot oxidation [25,26]. YSZ was selected as this material presents high chemical and thermal stability as demonstrated in sensors (Lambda sensors) and solid oxide fuel cells technologies, up to 1000 °C in both reducing and oxidizing atmospheres. Unlike ceria or perovskite catalysts, YSZ does not present any redox properties in diesel exhaust conditions; neither Zr^{4+} nor Y^{3+} can change their oxidation states. However, the partial substitution of Zr^{4+} with Y^{3+} creates oxygen vacancies in the cubic structure and provides a bulk oxygen ionic conductivity to YSZ whatever the gaseous atmosphere. This intrinsic oxygen conductivity gives rise to YSZ a catalytic activity for soot oxidation with oxygen. Using isotopic experiments, we have suggested a fuel-cell type electrochemical mechanism to explain the ignition of the soot oxidation. It is proposed that the soot is electrochemically oxidized with ionic O^{2-} species at the soot/YSZ interface (3 and 4), whereas YSZ is replenished via gas-phase oxygen electrochemical reduction at the triple phase boundary (tpb) gas/soot/YSZ (5). Electrons produced during carbon oxidation by ionic oxygen species O^{2-} are able to migrate to the reduction sites through the soot, with the last being not only a reactant but an electronic conductor as well.

$$C + 2\ O^{2-}_{(YSZ)} \rightarrow CO_{2\ (g)} + 4e\text{-}\ \text{(electron transfer through the soot)} \quad (3)$$

$$C + O^{2-}_{(YSZ)} \rightarrow CO_{\ (g)} + 2e\text{-}\ \text{(electron transfer through the soot)} \quad (4)$$

$$2\ O_{(ads)} + 4e^{-} \rightarrow 2\ O^{2-}_{(YSZ)} \quad (5)$$

As in fuel cells, the electromotive force of this process is the gradient of oxygen concentration between the tpb and the soot/YSZ interface. As YSZ is not a reducible oxide, soot oxidation must simultaneously take place with oxygen incorporation into the lattice, which is provided by the gas phase.

Soot oxidation over YSZ was *in-situ* observed by E-TEM (Environmental Transmission Electron Microscopy) and it was confirmed that the reaction takes place at the interface between the soot particle and the catalyst surface [27]. The soot/YSZ interface was observed to be 20–40 nm in length and the reaction appeared to be determined by the number of such contact points. Another limitation was found to be the kinetic of the incorporation of gaseous oxygen into YSZ (5). Therefore, we decided to associate YSZ with silver which known to be a good electrocatalyst for oxygen activation [28,29] due to its superior oxygen solubility and mobility. In addition, silver was also widely studied for soot oxidation [30–39]. Its activity is related to its mobility over the soot [40–43] along with its potential to form active oxygen species [30,33,34,39,44] such as peroxide and superoxide. For instance, Nanba et al. [44] showed that maximal activity toward soot oxidation was obtained for a loading of 5 wt% of Ag dispersed on ZrO_2. The activity is assumed to be correlated to the highest amount of active oxygen species available at the surface of finely dispersed Ag nanoparticles. The silver oxidation state was also studied, metallic particles were detected by XRD and both metallic silver species and cationic silver clusters were observed by UV–vis over highly-loaded Ag/ZrO_2. It is therefore possible that two types of particles co-existed, smaller metallic nanoparticles along with bigger particles containing both metallic (observed by XRD) and silver oxide (observed by UV–vis). We have recently shown [39] that the catalytic performance for soot combustion of Ag-modified perovskite mainly depends on the location and oxidation degree of Ag. The presence of surface Ag/AgOx nanoparticles seems to enhance the activity, as observed on silver-modified lanthanum manganite perovskites.

Soot oxidation by silver-supported catalyst was also carried out by Yamazaki et al. [33], who tested silver impregnated ceria (Ag/CeO_2) along with a specific “rice-ball” formulation displaying a metallic silver core covered by ceria nanoparticles. Maximal performances were observed for this latter formulation compared to conventional impregnated catalysts. They proposed that gaseous oxygen adsorbs and dissociates over the silver core and then migrates to ceria nanoparticles, forming O^{2-} active species. The active oxygen species concentration was supposed to be dependent on the silver/ceria interface, with a larger interface allowing for more numerous active oxygen species. Catalysts with intermediate Ag nanoparticle sizes of 35–40 nm were shown to produce greater amounts of active oxygen species.

The mobility of Ag nanoparticles during soot combustion processes was recently investigated with E-TEM. For instance, Gardini et al. observed soot oxidation by non-supported silver particles [43] *in situ* at 340 °C for O_2 partial pressures of 300 Pa. The reaction was found to occur by the “tunneling” of mobile silver particles into the soot; such mobility resulted in the coalescence of silver particles once the soot was fully consumed. Similar Ag nanoparticle mobility was observed by Mori et al. [42] on silver supported ceria at 300 °C in the presence of 1 Pa of O_2 (total pressure of 5 Pa). They reported that the oxidation reaction occurred mostly at the soot-silver/ceria interface. In addition, the Ag nanoparticles coalescence phenomenon was not observed.

The aim of this study is to investigate a potential synergy between Ag nanoparticles and YSZ. To study the combined effect of Ag and YSZ, we impregnated commercial YSZ with a silver nitrate solution at different contents. ICP, BET, XRD–v, XPS, and TEM characterizations were carried out to determine the loading, size and shape of the silver nanoparticles. The catalytic performances of the samples for soot combustion were tested under different soot-catalyst contact conditions to assess the mobility of silver, along with different O_2 partial pressures. Beyond the performances measurements, we studied the effect of silver on YSZ through isotopic experiments: labelling oxygen adsorption and exchange, CO_2 adsorption and exchange as well as isotopic oxidation of soot over Ag/YSZ.

2. Experimental section

2.1. Catalysts preparation and characterization

Commercial YSZ (8% mol yttria) was purchased from Tosoh company and wet impregnated with a silver nitrate aqueous solution obtained by the dissolution of $AgNO_3$ (Sigma Aldrich, purity 99%). Samples were evaporated and dried overnight at 100 °C then calcinated at 700 °C for 4 h in air. Several samples with different Ag contents (from 0.1 to 7.5 wt%) were prepared in the same way. Table 1 gives the list of the prepared Ag/YSZ catalysts and their nomenclature.

Silver loading was determined by ICP-OES using a Horiba Jobin Yvon Activa spectrometer. Specific surface areas (SSA) were estimated from N_2 adsorption at −196 °C (BET method), using a Tristar Surface Area and Porosity Measurement apparatus from Micromeritics. XRD diffractograms were recorded using a Bruker D8 Advance A25 diffractometer using Cu Kα radiation.

XPS spectra were only recorded for 1Ag with an AXIS Ultra DLD from Kratos Analytical using a monochromatized Al X-ray source (hv = 1486.6 eV). Scanning energy was 40 eV for every region. Peaks were referenced using C1S peak of carbon (BE = 284.6 eV). Samples were pretreated at 200 °C in He before measurements were taken.

All samples were observed by TEM using a JEOL 2010 microscope.

Table 1
List of the different Ag/YSZ catalysts.

Catalysts	%Ag (wt.)	Ag crystallite size (nm)[a]
0.1Ag	0.12	–
0.2Ag	0.20	–
0.4Ag	0.43	–
0.8Ag	0.75	–
1Ag	1.12	–
1.4Ag	1.43	49
2Ag	2.11	42
4Ag	4.00	42
7.5Ag	7.52	37

[a] Determined from XRD.

The acceleration voltage was 200 kV with a 0.2 nm resolution. Samples were previously dispersed in ethanol using an ultrasound bath. One drop of solution was then deposited on a copper grid.

2.2. Catalytic performance measurements

Performances toward soot oxidation were measured by running TPO (temperature-programmed oxidation) of a mixture of model soot (Printex U) and catalyst under 5% O_2/He and 1% O_2/He at 100 mL/min with the temperature increasing by 10 °C/min from room temperature to 750 °C. Two types of contact, denominated as "tight" and "loose", were obtained by either mixing the two powders together in a ball-mortar or with a spatula. "Tight" contact is generally used to assess the intrinsic activity of the catalyst toward soot oxidation as it maximizes the contact between the two, while "loose contact" is considered to be more representative of the poor contact quality obtained between a catalyst wash-coat and the particles trapped by the DPF [2,45]. TPO experiments were conducted twice to check the reproducibility. SiC powder mixed in both tight and loose contact with model soot was used to gain insight into the reactivity of the latter without the presence of a catalyst. The soot to catalyst ratio was ¼; therefore, 25 mg mixture was introduced in a U-tube quartz reactor. Outlet gases were analyzed by a micro-chromatograph from SRA, with the CO_2 concentration measured on-line with a Horiba IR analyzer. Soot to gas conversion was obtained by integration of the molar production rate of CO and CO_2 with respect to time during soot oxidation experiments followed by normalization with respect to the total amount of soot initially present in the reactor.

2.3. Temperature-programmed Isotopic exchange (TPIE)

TPIE experiments were performed using 200 mg of catalyst introduced in a U-shaped reactor. Labelled O_2 (97.1% ^{18}O, 0.8% ^{17}O, and 2.1% ^{16}O), obtained from EURISOTOP, was diluted in He to obtain a flux of 1% $^{18}O_2$/He, which was introduced in the reactor at 75 mL/min. Samples were heated at 5 °C/min from room temperature to 700 °C and outlet gases were analyzed with a Hiden quadrupole mass spectrometer. Signals *m/z* followed were 32, 34 and 36, and signal calibration was performed with a 1% $^{16}O_2$/He (99.99% purity) calibration bottle provided by Linde. A blank experiment in the presence of both 1% $^{16}O_2$ and $^{18}O_2$ in the reactor was performed without any catalyst to check that gaseous homoexchange does not take place until 700 °C.

Molar fractions of O_2 were calculated following equation (6):

$$F_{32} = C_{32} / (C_{32} + C_{34} + C_{36}) \quad (6)$$

Where F is an isotopomer molar fraction and C_{32}, C_{34} and C_{36} are the respective concentrations of the three O_2 isotopomers detected during the reaction.

The consumption rate of labeled oxygen ($^{18}O_2$) and the production rate of normal oxygen ($^{16}O_2$) were calculated at a given temperature T using the following equations (7 and 8):

$$R_{C,\,T} = F^*(F36_{\,in,T} - F36_{out,T})/V_m \quad (7)$$

$$R_{P,\,T} = F^*(F32_{\,out,T})/V_m \quad (8)$$

Where F (L/s) is the total flow rate, and $F36_{\,in,T}$ and $F36_{\,out,T}$ are the labeled oxygen molar fraction in the flow at the reactor's inlet and outlet at temperature T, respectively. $F32_{\,out,T}$ is the outlet molar fraction of oxygen at temperature T and V_m is the molar volume at the temperature of the MS analysis. If no $^{16}O^{18}O$ oxygen species are present in the gas phase at the temperature T and if $R_{C,T} = R_{P,T}$, then the value of these equal rates gives the surface oxygen exchange rate of the catalyst.

Isothermal oxygen exchange (IOE) experiments were also conducted with $C^{16}O_2$ over previously exchanged samples with labeled oxygen: 20 mg of catalyst was exposed to 30 mL/min of 1% $^{18}O_2$/He at 650 °C until complete exchange of ^{16}O bulk oxygen species (until no more $^{16}O_2$ or $^{18}O^{16}O$ species were detected in the gas phase) and cooled down to room temperature. The so-called ^{18}O-exchanged catalysts were then heated in He at 400 °C and 550 ppm $C^{16}O_2$/He was introduced into the reactor at 100 mL/min. Isotope concentrations were measured with the same Hiden quadrupole mass spectrometer. Signals *m/z* followed were 32, 34 and 36 for oxygen isotopes and 44, 46 and 48 for CO_2 isotopes. Prior to each experiment, the signal was calibrated using 2000 ppm $C^{16}O_2$/He and 1% $^{16}O_2$/He calibration bottles provided by Linde. CO_2 isotopomer molar fractions were calculated using (9):

$$F_{44} = C_{44} / (C_{44} + C_{46} + C_{48}) \quad (9)$$

Where F_{44} is an isotopomer molar fraction and C_{44}, C_{46} and C_{48} are the respective concentrations of the three CO_2 isotopomers detected during the reaction.

The total amount of carbon was calculated by integrating the molar rate of total CO and CO_2 produced during the experiment. A comparison was made with initial amounts of carbon in the reactor to assess carbon balance.

2.4. Isotopic soot oxidation

Isotopic soot oxidation was performed using 25 mg of a mixture of Printex U and catalyst with a mass ratio of 1/4, under both tight and loose contacts. Then, 1% $^{18}O_2$/He was obtained as described above and introduced to the reactor at 75 mL/min. The temperature was raised at 5 °C/min from room temperature up to 750 °C. Signals *m/z* followed, with the same Hiden quadrupole mass spectrometer, were 32, 34 and 36 for oxygen isotopes, 28 and 30 for CO isotopes as well as 44, 46 and 48 for CO_2 isotopes. Prior to each experiments, signal was calibrated using 2000 ppm $C^{16}O_2$/He and 1% $^{16}O_2$/He calibration bottles provided by Linde. The total amount of oxidized carbon was calculated from the integration of molar flow rates of total gaseous CO_2 and CO. Calculated amounts of carbon were compared to the real amount of soot present in the reactor (5 mg). Variations between calculated amount and introduced amount of carbon remained below 10%.

3. Results and discussion

3.1. Catalyst characterizations

Various samples were prepared following the impregnation-calcination method (Table 1). XRD diffractograms obtained for all catalysts are displayed in Fig. 1. YSZ displays a characteristic cubic fluorite structure while silver is only detected as metallic for high contents. No evidence for the presence of AgO_x or $Ag\delta^+$ crystallites was observed. The main diffraction peak of the (100) plan of metallic silver was detected at 38.1°, starting at 1 wt% Ag loading. Peak resolution allows crystallize size calculation by the Scherrer method only from 1.4%Ag loading and beyond. The average silver particle size appears to be around 40 nm (Table 2); similar crystallite sizes were obtained for silver-impregnated zirconia [38,44] and ceria [33] calcined at

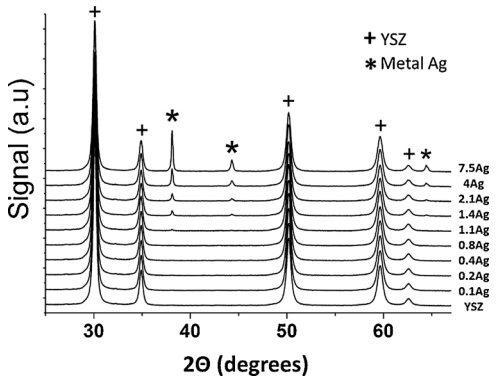

Fig. 1. XRD patterns of Ag/YSZ catalysts.

temperatures between 500 and 600 °C. Let us note that the calcination temperature of our samples (700 °C) is higher than those used in the literature, generally ranging from 400 °C to 600 °C. This can probably promote the sintering of silver nanoparticles. In addition, YSZ displays a rather low specific surface area (SSA) of only 12 m^2/g (Table 2). Nonetheless, thermal treatment does not seem to impact YSZ support as the SSA of 1Ag is quite similar to that of the non-calcined bare support.

XPS analysis was performed on 1Ag without any specific pretreatment. The results show that the Ag concentration on the extreme surface is much higher than that in the volume (Table 2). One can conclude that silver is mainly located on the YSZ surface, which is in good agreement with the low porosity of the support. The atomic ratio Y/Zr appears to be heterogeneous as there are 30% more Y atoms on the surface than in the bulk (Table 2). The Y/Zr surface to volume atomic ratio evidences a segregation of yttrium at the surface, as already reported on YSZ purchased by Tosoh [46]. This could result in the enhancement of the surface oxygen vacancies concentration (Zr^{4+} substituted by Y^{3+}) which tends to increase the Lewis basicity [47].

The XPS signal (Fig. S1) of Ag $3d_{5/2}$ is centered at a binding energy of 367.0 eV with a shoulder at 368.4 eV. Binding energies related to silver oxide species are generally found at 367.4 eV (AgO) and 367.8 eV (Ag_2O), while for metallic silver it is shifted toward higher energies (368.1 eV). Therefore, the surface of the Ag particles seems to be predominantly oxidized. As the average silver particle size is 40 nm according to XRD data, one can assume that the top layer of the nanoparticles is mainly composed of silver oxide. During the preparation procedure, 1Ag was annealed in air at 700 °C and also cooled-down in air, thus producing silver oxide, which is stable at room temperature. Liu et al. [48] have also used XPS to analyze silver supported over various ceria supports presenting different morphologies (nanocubes, nanoparticles and spindles). Samples were calcined at 500 °C for 3 h under static air, instead of 700 °C in our study and, as expected, contained smaller nanoparticles in the range from 1.5 to 3.5 nm. All displayed an Ag $3d_{5/2}$ binding energy of 368.1 eV, indicating only metallic silver at the surface. Contradictory results were reported by Skaf et al. [49] on silver-impregnated ceria materials annealed at 400 °C for 1 h, which were therefore theoretically composed of highly dispersed nanoparticles. XPS spectra have shown an Ag $3d_{5/2}$ binding energy peak centered at 367.7 eV corresponding to Ag^+ ions with a smaller shoulder at 368.1 eV related to metallic silver.

TEM observations were conducted on all catalysts, except 0.1Ag and 0.2Ag, for which it was not possible to detect Ag nanoparticles. Silver particles ranging from 1 to 50 nm in diameter were detected (Fig. 2a), showing a wide size distribution. Statistics on size distribution were achieved over an average of 20 micrographs per catalyst. For each sample, 150 or more silver nanoparticles were counted and measured to obtain the size distribution displayed in Fig. 2b. TEM micrographs display silver particles of spherical shape with various diameters. However, contrast between YSZ and silver particles is rather poor due to the similar atomic numbers of Ag and Zr. Therefore, small Ag particles located at the periphery of the YSZ grains are preferentially detected, whereas bigger ones (over 25 nm) are hidden by YSZ grains. Therefore, all catalysts most probably exhibit two different average AgNP (NP: NanoParticle) size distributions. TEM observations mostly detect small AgNPs in the range from 8 to 12 nm, whereas XRD data have reported larger NPs in the range from 30 to 50 nm (Table 1). The AgNP size range observed by TEM is 8–12 nm, with the exception of 0.8Ag which displays a large quantity of 6 nm size particles; this is in good agreement with the data found in the literature [30] [31] [32]. Indeed, the Ag particle size in the range 10–20 nm over supports such as ZrO_2, Al_2O_3, SiO_2 and CeO_2 has been reported after calcination steps at 500 °C. As already observed with XRD, higher silver loading does not seem to correlate with larger Ag particles, suggesting a good thermal resistance of the AgNPs after the calcination step at 700 °C. We suggest that until 7.5% Ag, a higher loading might simply result in a higher surface density of particles.

3.2. Catalyst performances toward soot oxidation

Fig. 3 displays conversion versus temperature during the TPO of 1Ag, YSZ and SiC powders in both contact modes with the model soot (Printex U). SiC is commonly used as the main constituent of a DPF structure and is inert toward soot oxidation, thus allowing the study of the oxidation of non-catalyzed Printex U. As displayed in Fig. 3 and already shown by our group [25,26] YSZ is active for soot oxidation in tight contact mode, decreasing the T_{50} value (temperature corresponding to 50% soot oxidation) by 90 °C. However, when the soot/YSZ contact surface becomes limited (loose contact mode), YSZ is not able to activate the soot anymore, demonstrating again that combustion takes place at the solid/solid interface. The catalytic performance drop of YSZ is particularly pronounced because the YSZ powder contains large spherical agglomerates with diameters in the range from 20 to 160 µm [26], which strongly limits the contact with soot nanoparticles. The presence of 1 wt% silver over YSZ promotes soot oxidation, as displayed by the shift toward lower temperature in tight contact mode. The value of T_{50} diminishes by 60 °C between YSZ and 1Ag. More interestingly, in loose contact mode, the ignition of the soot combustion starts at temperatures lower than 400 °C and the T_{50} value is shifted by 100 °C in presence of 1 wt% Ag. In 1Ag, the tight contact soot conversion profile displays a more severe slope than in loose contact, which could be attributed to a higher number of contact points between the soot and the catalyst, hence promoting the propagation of the reaction. CO

Table 2
SSA and XPS data for YSZ and 1Ag.

Catalysts	Specific surface area (m^2/g)	Pores diameter (nm)	Porous volume (cm^3/g)	Atomic %Ag Volume[b]	Atomic %Ag Surface[c]	Y/Zr surface to volume atomic ratio
YSZ[a]	13	15	0.053	–	–	1.4
1Ag	12	12	0.040	1.6	2.1	1.3

[a] As provided, before impregnation and calcination at 700 °C.
[b] From ICP analysis.
[c] From XPS data.

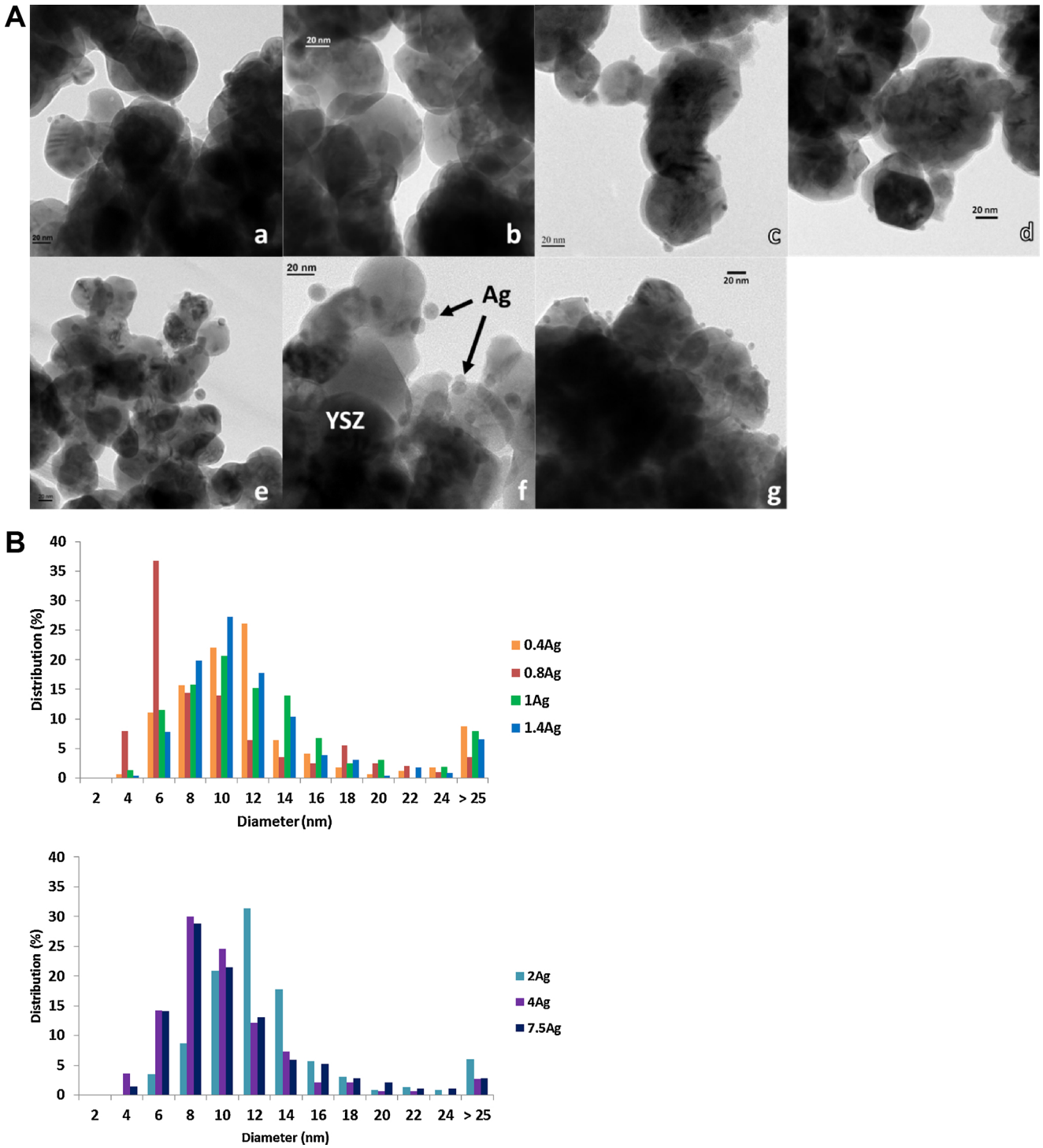

Fig. 2. TEM micrographs of Ag/YSZ catalysts, scale is 20 nm, a) 0.4Ag, b) 0.8Ag, c) 1Ag, d) 1.4Ag, e) 2Ag, f) 4Ag, g) 7.5Ag. Silver particles diameter distribution for Ag/YSZ catalysts (Ag loading from 0.4 to 7.5%) obtained from TEM observations.

selectivity is highly dependent on the contact mode, reaching 55% with bare YSZ in loose contact and only 10% in tight contact. In the case of 1Ag, no CO was detected in either contact mode. Such results correlate with high silver activity for CO oxidation, as reported in the literature [50–52].

The stability of the catalyst was studied by running three successive TPO experiments with a batch of catalyst. Here, 1Ag was mixed with soot in tight contact mode and this mixture was oxidized in TPO up to 750 °C. The process was repeated 3 times by using the same batch of 1Ag catalyst without any modification of the catalytic performances. ICP analysis to titrate Ag was conducted on a small amount of catalyst after each TPO. No silver loss was detected between some experiments, showing the thermal stability of Ag nanoparticles up to 750 °C. In addition, a TPO experiment in tight contact mode was performed with 10% H_2O in the feed (Fig. S2). As expected, the addition of H_2O decreases the soot oxidation activity of 1Ag. However, the value of T50 (temperature at 50% of soot conversion) slightly increases from 510 °C to 540 °C.

The impact of silver loading on the catalytic performances has been investigated in both contact modes. Fig. 4 displays variations in T_{10} and

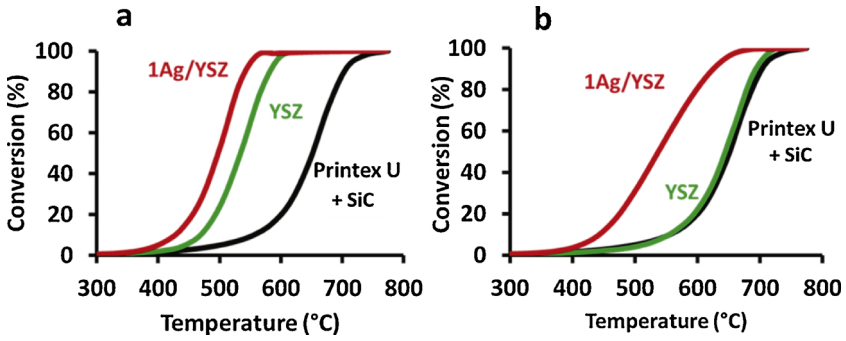

Fig. 3. Soot conversion versus temperature during TPO of 1Ag, YSZ and SiC mixed with Printex U soot a) in tight and b) in loose contact under 5% O_2/He at 6 L/h.

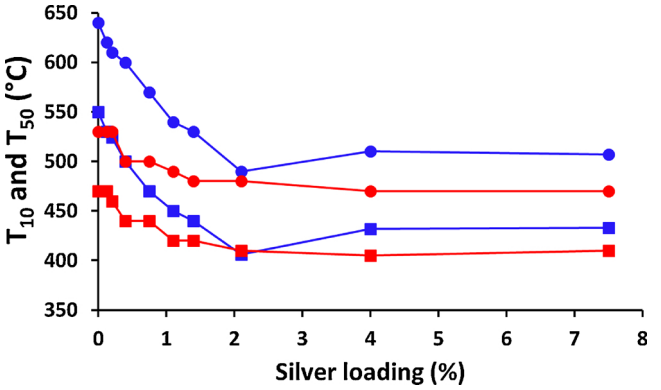

Fig. 4. Variations of T_{10} (square) and T_{50} (circle) values in loose contact (blue) and tight contact (red) as a function of the Ag loading during TPO under 5%O_2/He. (For interpretation of the references to colour in this figure legend, the reader is referred to the web version of this article.)

T_{50} values, indicating temperatures at 10 and 50% soot conversion, respectively, as a function of the silver loading. The parameter T_{10} mainly refers to the ignition of the catalytic soot combustion while T_{50} is a good indicator of the thermal oxidation due to exothermic effects. In tight contact mode, the addition of Ag starts to significantly improve the catalytic performances from 0.4 wt%, whereas 2 wt% seems to be sufficient to reach the lowest values of T_{10} and T_{50}. For loose contact mode, performances are already improved from low contents until 2 wt % of Ag. Furthermore, the impact of Ag is much more pronounced in loose contact mode. For instance, the T_{10} decrease in the presence of Ag reaches 150 °C in loose contact mode and only 60 °C in tight contact mode. For Ag contents larger than 2 wt%, performances become either similar or slightly lower even in loose contact mode. Similar trends were reported in the literature [30,33,44], with silver-supported zirconia and ceria catalysts calcined at 500 °C. Optimal catalytic performances were obtained for 5%wt silver loading, and started to decrease at higher loading performances. Nanba et al. [44], who studied Ag/ZrO_2 catalysts, reported that the amount of active oxygen available was maximum for a loading of 5 wt% silver, thus leading to the highest activity. In this work, the calcination temperature was higher (700 °C), making it possible for more severe sintering to occur, shifting the maximal activity toward lower loading, i.e. 2%wt.

In both contact modes, CO is only detected for silver contents lower than 0.4 wt%. In loose contact mode, CO selectivity drops from 55% over bare YSZ to 40, 20 and 3% over 0.1Ag, 0.2Ag and 0.4Ag, respectively. Therefore, 0.4 wt% Ag loading is sufficient to avoid CO emissions in our operating conditions.

Oxygen partial pressure effect was also investigated by running TPO in tight contact mode under 1% O_2/He instead of 5%. Whatever the catalyst, performances drop along with lower oxygen partial pressure (Fig. 5). When decreasing the oxygen partial pressure from 5% to 1%, T_{10} and T_{50} values significantly increased in the ranges from 40 to

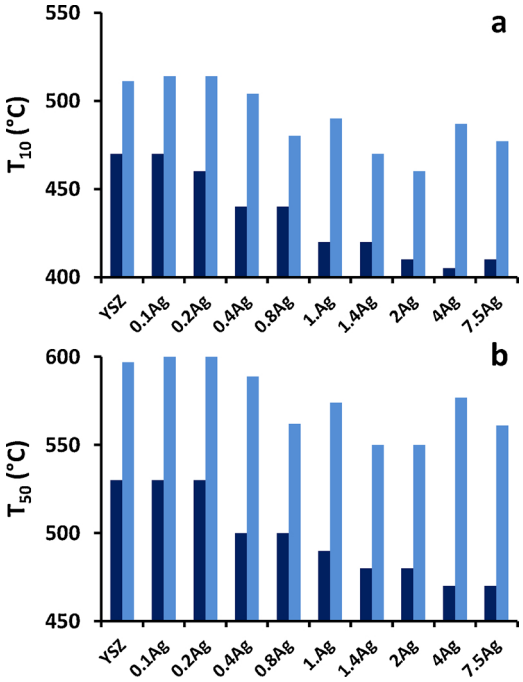

Fig. 5. a) T_{10} and b) T_{50} values obtained during TPO in tight contact under 5% O_2/He (dark blue bars) and 1% O_2/He (blue bars). (For interpretation of the references to colour in this figure legend, the reader is referred to the web version of this article.)

80 °C, and 60–100 °C, respectively. It is interesting to note that the drop in performance is more pronounced for high Ag contents. For instance, the difference between T_{10} values recorded at 1% and 5% O_2 was found to be only 40 °C for YSZ and 70 °C for 1Ag. Therefore, the role of Ag in the activity enhancement is not only due to the improvement in the soot/catalyst contact surface through its mobility. This series of TPO with low oxygen partial pressure clearly demonstrates that AgNPs are involved in the activation of gaseous oxygen. The lowest oxygen dependence on the performance was observed for 0.8Ag, which is the material with the highest Ag dispersion according to TEM results (Fig. 2b). Without oxygen in the gas phase (TPO with only He in the gas phase), no soot oxidation was observed, which correlates to similar experiments performed by Obeid et al. over bare YSZ [26]. Even in the presence of Ag on its surface, YSZ cannot be reduced in these operating conditions and release bulk oxygen species for soot oxidation.

3.3. Temperature-programmed isotopic exchange of oxygen

To assess the effect of silver on oxygen surface exchange, we performed TPIE experiments with labelling O_2 both over YSZ and 1Ag, which was found to be one of the most active catalysts. Oxygen

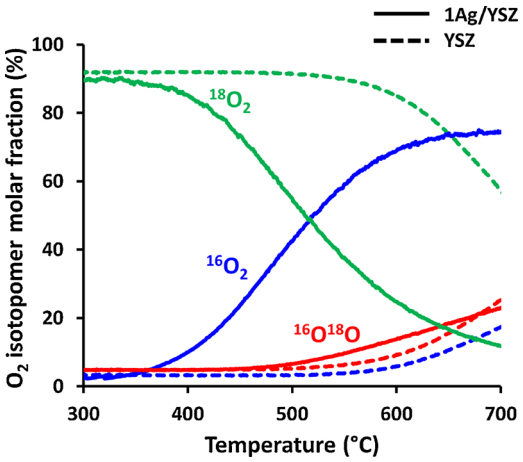

Fig. 6. TPIE experiments on YSZ (dashed line) and 1Ag (solid line), 1% $^{18}O_2$/He, flow rate is 75 mL/min. Green: m/z = 32, red: m/z = 34, blue: m/z = 36. (For interpretation of the references to colour in this figure legend, the reader is referred to the web version of this article.)

exchange was observed while heating the sample under 1% $^{18}O_2$/He. The evolution of oxygen isotope molar fractions with respect to temperature is displayed in Fig. 6. Small initial molar fractions of 32 and 34 isotopes are due to traces of ^{16}O and ^{17}O in the $^{18}O_2$ gas cylinder.

On YSZ, the surface oxygen exchange between gaseous $^{18}O_2$ and YSZ bulk oxygen species only takes place from 550 °C and simultaneously produces both 32 and 34 species. On 1Ag, the oxygen exchange is shifted by 200 °C, starting from 340 °C with a unique initial production of $^{16}O_2$ until 480 °C. The oxygen exchange mechanism is described in the literature [53–56] according to a simple (10) or multiple (11) heteroexchange, involving either one or two oxygen atoms of the catalyst. The initial production of $^{16}O^{18}O$ and $^{16}O_2$ in the gas phase allows these two possible processes to be discriminated between. For YSZ, 32 and 34 oxygen species are simultaneously desorbed in the gas phase. This indicates that simple and multiple mechanisms of oxygen exchange occur on YSZ. On the contrary, for 1Ag, the initial product of the exchange is $^{16}O_2$ alone, showing that only multiple heteroexchange is taking place. This clearly demonstrates that oxygen exchange only occurs on Ag nanoparticles below 500 °C.

$$^{18}O^{18}O(g) + {}^{16}O(s) \rightarrow {}^{18}O^{16}O(g) + {}^{18}O(s) \quad (10)$$

$$^{18}O^{18}O(g) + 2\,{}^{16}O(s) \rightarrow {}^{16}O_2(g) + 2\,{}^{18}O(s) \quad (11)$$

Table 3 displays the total amount of exchanged oxygen during TPIE experiments, as well as the fraction of lattice oxygen exchanged. On YSZ, only 0.7% of the overall oxygen atoms have been exchanged, while almost 10% were exchanged on 1Ag at the end of the TPIE. At both 450 and 500 °C, where F34 is negligible, the $^{18}O_2$ consumption rate is 20 times higher in the presence of 1 wt% silver (Table 3), confirming that, in this temperature range, the oxygen exchange is predominantly taking place on Ag nanoparticles. These results underline that Ag nanoparticles strongly promote oxygen activation, most probably by boosting the molecular oxygen dissociative adsorption step.

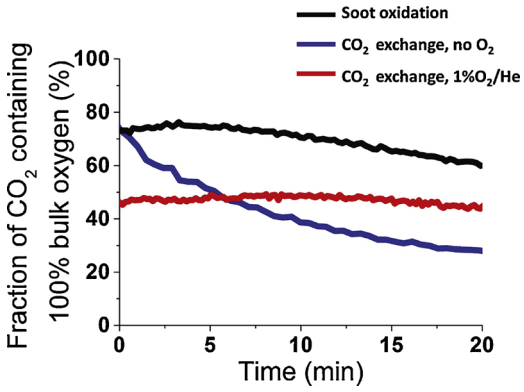

Fig. 7. Fraction of CO_2 containing only bulk oxygen species during isothermal soot oxidation under 1%O_2/He (black), CO_2 exchange without O_2 (blue), CO_2 exchange under 1%O_2/He (red) at 400 °C for 1Ag. (For interpretation of the references to colour in this figure legend, the reader is referred to the web version of this article.)

3.4. Isothermal oxygen exchange experiments

To elucidate the role of lattice oxygen species in the soot oxidation mechanism, this reaction was implemented with labeled oxygen on YSZ and 1Ag in both tight and loose contact modes with the model soot. First, the oxygen exchange activity from CO_2 was investigated, as this is the main reaction product of the soot combustion and may induce oxygen exchange via carbonate formation [57–60]. During isotopic experiments at 400 °C in the presence of CO_2 (500 ppm in He) and CO_2/O_2 (500 ppm/1% in He), we observed oxygen exchange over YSZ and 1Ag (Figs. S3 and S4), mainly through surface carbonation. Such phenomena have been reported in the literature over various oxides in the presence [57,58] or absence [59,60] of precious metals and also over silver crystals [61]. However, it has never been reported during soot combustion with labeled oxygen. These results emphasize that the CO_2 produced by soot combustion can strongly participate in the oxygen exchange process. Therefore, understanding of the soot oxidation mechanism may be polluted by this oxygen exchange from CO_2. A detailed investigation is needed to clearly highlight the key role of YSZ bulk oxygen species. Fig. 7 displays the amount of CO_2 isotopes containing two lattice oxygen atoms during soot oxidation, as well as during CO_2 exposure experiments on 1Ag. The latter were undertaken with and without oxygen in the gas phase. All of these experiments were performed at 400 °C. Soot oxidation was conducted with $^{18}O_2$ in the gas phase and ^{16}O in the YSZ bulk, whereas $C^{16}O_2$ with and without $^{16}O_2$ was introduced on 1Ag, previously exposed to $^{18}O_2$ (Fig. S4). Soot oxidation and CO_2 exposure without oxygen initially produce similar amounts of CO_2 (75%) containing two oxygen atoms from the YSZ bulk. However, in the latter case, the production quickly drops to 40% over the first 10 min. In the presence of oxygen, CO_2 introduction only produces 45% of double-exchanged species. It appears that a rather large portion of produced CO_2 containing two lattice oxygen during soot oxidation could not be only explained by the process of oxygen exchange via CO_2. Hence, despite the presence of mobile Ag

Table 3
Oxygen exchanged during TPIE for YSZ and 1Ag.

	Amount of exchanged oxygen (μmol)	Fraction of lattice (^{16}O) exchanged oxygen (%)	Consumption rate R_c of $^{18}O_2$ at 450 °C (atoms/$g_{catalyst}$/s)	Consumption rate R_c of $^{18}O_2$ at 500 °C (atoms/$g_{catalyst}$/s)
YSZ	22	0.7	1.4×10^{16}	2.4×10^{16}
1Ag	298	9.8	30×10^{16}	54×10^{16}

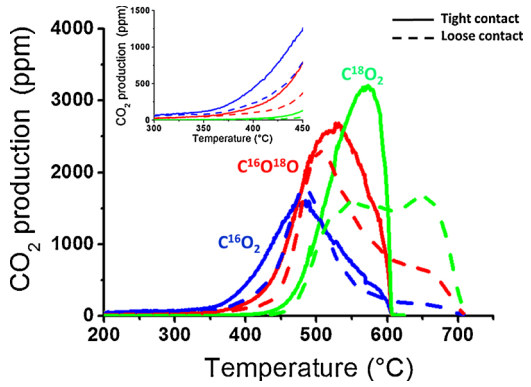

Fig. 8. Isotopic CO_2 production with respect to temperature during isotopic TPO of 1Ag mixed with Printex U in tight contact (solid line) and loose contact (dashed line) modes. $C^{16}O_2$ (blue), $C^{16}O^{18}O$ (red), $C^{18}O_2$ (green). 1% $^{18}O_2$/He, 75 mL/min, 5 °C/min. (For interpretation of the references to colour in this figure legend, the reader is referred to the web version of this article.)

nanoparticles, the soot ignition process at 400 °C preferentially involves the YSZ lattice oxygen which would imply that these species are more active toward soot oxidation than gaseous ones, as shown in our previous study on bare YSZ [25].

3.5. Temperature-programmed oxidation of soot with labeled oxygen

We investigated the soot oxidation mechanism by running isotopic TPO for a mixture of 1Ag and Printex U in loose and tight contact modes under 1% $^{18}O_2$/He (Fig. 8). Under both types of contact, soot oxidation produces first $C^{16}O_2$, followed by $C^{16}O^{18}O$ and finally $C^{18}O_2$, which is in good agreement with a previous study on bare YSZ [25,26]. It is interesting to note that the isotopes produced are similar for the two types of contact modes, although shifted toward higher temperatures for loose contact. However, the zoom in Fig. 8 shows that, regardless the quality of the contact, the ignition of soot combustion starts at similar temperatures, close to 350 °C. The lower concentrations of $C^{16}O_2$ observed for the loose contact mode are probably due to fewer solid/solid contact points between soot and the catalyst surface. The CO_2 production shoulder between 600 °C and 700 °C in loose contact is related to the oxidation of soot particles that are not in contact with the catalyst (thermal oxidation). Hence the majority of the CO_2 produced in this temperature region is $C^{18}O_2$. Cross-labeled $C^{16}O^{18}O$ and $C^{18}O_2$ are probably produced by CO_2 exchange over the catalyst surface and with bulk ^{18}O species previously incorporated at the beginning of TPO. The total amounts of bulk oxygen species involved in the CO_2 production during TPO were found to be 15.2 and 14.7 mmoles/g in tight and loose contact modes, respectively. The results are slightly lower in the loose contact mode because of the fraction of soot that is not in contact with the catalyst and consumed through thermal oxidation. Upon full oxidation of the soot, almost 100% of the initial ^{16}O lattice oxygens were consumed (15.2 mmoles/g catalyst). The maximum exchanged amount of lattice oxygens during TPO of the same amount of soot on bare YSZ was reported to be 60% in the tight contact mode [26]. This confirms that silver promotes oxygen exchange and then activates oxygen transfer from the lattice to the soot, leading to an increase of ^{16}O in the CO_2 produced.

4. Discussion

A series of silver-impregnated YSZ catalysts was prepared by wet impregnation followed by calcination at 700 °C. Catalysts displayed silver loading ranging from 0 to 7.5 wt%. AgNPs have a bimodal size distribution at around 10 and 40 nm, as deduced from TEM and XRD analysis. Significant activity improvement was observed in loose contact mode for silver contents as small as 0.1% with maximal performances found for 2 wt% samples. Similar optimum Ag loading was observed in tight contact mode. Trends in the literature display maximal activity for higher Ag contents, typically 5 wt% on ZrO_2 or CeO_2 supports [30,33,44]. For instance, Aneggi et al. [30] reported optimal performances for 5 wt% silver loading for AgNPs dispersed on ceria or zirconia for both calcined (500 °C) and aged (850 °C) samples. It is interesting to note that SSA of the aged samples is similar to that of our YSZ-supported catalysts, i.e. between 12 and 19 m^2/g. No silver loss was recorded upon cycled TPO up to 750 °C, indicating the high thermal stability of the catalyst. Therefore, the low optimal Ag loading achieved on YSZ cannot only be explained by specific interactions between YSZ and Ag NPs. Recently [62], a Au/ZnO composite containing only 1 wt% Au was found to exhibit an excellent activity for soot oxidation that was explained by a strong interaction between gold and ZnO.

The silver chemical nature involved in the soot combustion process is still under debate in the literature, but most of the recent studies consider metallic AgNPs as active sites, as AgOx species decompose above 189 °C according to the Ellingham diagram. Machida et al. [63] propose that the metallic surface Ag promotes the formation of superoxide ions O_2^- that might assist carbon oxidation. This result was confirmed by Corro et al. for soot oxidation over silver-loaded SiO_2 [31]. Silver particles were shown to be reduced after reaction and higher activity was measured for reduced samples containing only metallic silver particles. Silver-supported silica activity was shown to be stable after 6 soot oxidation cycles up to 600 °C, indicating that metallic silver particles remain well-dispersed, which correlates with the absence of silver loss detected in this study. Shimizu et al. studied soot oxidation over Ag/CeO_2 and proposed that ceria surface vacancies are involved into the formation of O_2^- from adsorbed gaseous oxygen [36]. According to these authors, the role of AgNPs would be to promote both the oxidation and reduction of ceria, allowing vacancies to be easily produced. As no CO was detected during soot oxidation over Ag/CeO_2, Shimizu et al. assumed that soot is directly oxidized to CO_2 by O_2-. Another route would be the high activity of AgNPs toward CO oxidation [50], implying that soot oxidation produces CO, which reacts immediately over silver nanoparticles.

The silver oxidation state of AgNPs supported on YSZ appears to be mainly metallic, as indicated by XRD. XPS spectra indicate the presence of silver oxide on the surface, which can be associated with silver oxide shelled particles containing a metallic core, as proposed by Zhao et al. [64]. XPS results seem to be in contrast to the assumption considering metallic AgNPs as active sites for soot combustion. However, these characterizations were performed in ultra-high vacuum and are possibly not representative of the Ag chemical nature during the soot combustion process, as silver oxides are not thermally stable. This could also explain the assumptions of Haneda and Towata [65], for soot oxidation over the Ag/ZrO_2 catalyst. They proposed that oxygen species were activated on Ag^+ sites, but only *ex situ* techniques such as XPS and FT-IR spectra of CO adsorption have been used to support these hypotheses. They have also performed isothermal isotopic soot oxidation experiments at 320 °C. Gaseous oxygen was switched from $^{16}O_2$ to $^{18}O_2$ during the reaction, leading to $C^{16}O^{18}O$ being produced first and in larger quantities, followed by $C^{18}O_2$. The authors concluded that oxygen species were formed on Ag^+ sites from gaseous oxygen and reacted directly with the soot. However, according to our results, the initial production of $C^{16}O^{18}O$ is a clear indication of a mechanism of oxygen exchange driven by the zirconia surface carbonation (Fig. S4), as already reported for bare ZrO_2 [60]. We have shown in Fig. 7 that CO_2 exchange occurred at low temperatures and could be considered an artefact when performing isotopic soot oxidation. This underlines that the oxygen mechanism via surface carbonation must be carefully analyzed to clearly conclude the origin of the active oxygen species. Isothermal oxygen exchange experiments performed at 400 °C with labeled oxygen on YSZ [26] and 1Ag in both tight and loose contact modes with the model soot clearly show that the largest amount of lattice oxygen is

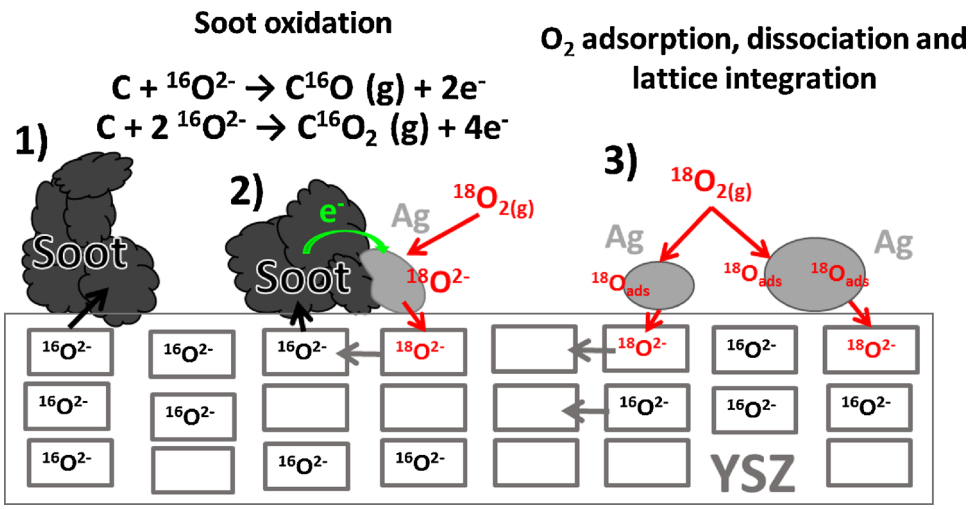

Fig. 9. Mechanism for soot ignition by 1Ag/YSZ, oxidation of soot to CO and CO_2 on YSZ (1) and in contact with Ag (2), O_2 adsorption and dissociation over silver particles (3).

detected in the CO_2 produced during the first 20 min of the soot combustion process in comparison with the CO_2 route exchange. This indicates that YSZ bulk oxygens are largely involved in soot oxidation (Fig. 8). The formation of active oxygen directly on Ag nanoparticles from the gas phase does not seem to occur as no $C^{18}O_2$ is detected during the first minutes of isotopic soot oxidation (Fig. 8). Similarly, no significant production of CO_2 was detected during soot oxidation over 1Ag/YSZ under He, indicating that negligible active oxygen species were available. Furthermore, in the tight contact mode, Ag contents up to 0.4 wt% have no significant effect on the catalytic performance, showing that when the soot/YSZ contact is good, YSZ can provide active oxygen species to oxidize soot. Nanba et al. observed different results over an Ag/ZrO_2 catalyst mixed with soot [66]. Two CO_2 peaks (350 °C and 400 °C) were detected when heating a mixture of catalyst and soot in He. Mixture was pretreated in He at 250 °C to remove adsorbed CO_2 and then flushed with O_2 at ambient temperature. The authors concluded two kinds of active oxygen species co-existed over the catalyst surface. Differences to our results might be explained by the larger amount of catalyst used by Nanba et al. (1/100 soot to catalyst ratio against ¼ in the present study). Oxygen partial pressure was shown to impact performances (Fig. 5); the activity drop when decreasing the oxygen partial pressure from 5 to 1% was found to be stronger in the presence of silver than over bare YSZ, thus indicating that silver plays a role into oxygen replenishment. As YSZ is not reducible, soot oxidation must involve the integration of gaseous oxygen into the lattice to replace lattice oxygens consumed to oxidize soot. The replenishing of YSZ with oxygen corresponds to the electrochemical reduction of oxygen. This is most probably the rate-determining step of the overall combustion process, as in solid oxide electrochemical devices [67]. This replenishing of YSZ is promoted by AgNPs, as confirmed by TPIE. The presence of AgNPs on YSZ strongly promotes the oxygen dissociative adsorption, as well as its integration into the YSZ lattice (Fig. 6). As shown in Fig. 6, the decrease in the $^{18}O_2$ partial pressure in the gas phase is simultaneously compensated by the release of $^{16}O_2$ from YSZ bulk. Such a result correlates with the high performance of silver as an electrode for gaseous oxygen reduction, as discussed by Sun et al. [67].

Soot/catalyst contact is a limiting parameter for soot combustion [68]. Isotopic TPO experiments of soot have shown that whatever the quality of the contact, the ignition of soot combustion starts at similar temperatures, close to 350 °C. Lower catalytic rates observed for loose contact mode are probably due to a limited number of solid/solid contact points between soot and the catalyst surface. AgNPs have also shown to increase performances in loose contact (Fig. 3) for contents as small as 0.1 wt% (Fig. 5). This suggests that a small quantity of AgNPs well dispersed on YSZ may enhance the surface contact between soot and YSZ.

To account for the various phenomena occurring over silver-promoted YSZ during soot oxidation, we propose the following mechanisms (Fig. 9):

- Soot oxidation occurs through bulk O^{2-} YSZ oxygen species being provided to soot particles, either by a synergy between Ag and YSZ or by YSZ directly when no silver particles are present, as described by Obeid et al. [26]. The replenishment of depleted oxygen mostly occurs below 500 °C at the triple phase boundary gas/Ag/YSZ. AgNPs promote gaseous oxygen dissociative-adsorption along with integration into the YSZ lattice. YSZ ionic conductivity allows for the transfer of active species from the bulk to the interface with the soot. The rate-determining step of this process could be the replenishment of YSZ by oxygen, a step which is strongly accelerated by AgNPs.
- The nature of the active oxygen species coming from the YSZ bulk has not been investigated in this study. The absence of CO production indicates that superoxide ions could be produced from O_2^- YSZ bulk species:

$$C + O_2^- \rightarrow CO_2 + e- \quad (12)$$

However, CO can be also oxidized over AgNPs, suggesting that active oxygens originate from the YSZ lattice (O^{2-}):

$$C + O^{2-} \rightarrow CO + 2e- \quad (13)$$

$$CO + O^{2-} \rightarrow CO_2 + 2e- \quad (14)$$

- Once soot is oxidized and CO_2 is produced, surface oxygen exchange can occur by carbonation over Lewis sites.

5. Conclusion

We investigated soot oxidation over bare YSZ and silver-supported YSZ through TPO and isotopic experiments. Ag/YSZ displays high thermal stability and maximal activity for low loading of Ag (2 wt%) thanks to the ability of silver to disperse into small metallic nanoparticles. We evidenced the interference of produced CO_2 during soot oxidation in the oxygen exchange process and then performed suitable experiments to prove that active oxygen species originate from the YSZ lattice. Silver was shown to promote soot oxidation activity by

activating the dissociative adsorption and lattice integration of gaseous oxygen.

Appendix A. Supplementary data

Supplementary material related to this article can be found, in the online version, at doi:https://doi.org/10.1016/j.apcatb.2018.09.069.

References

[1] B.T. Johnson, Platin. Met. Rev. 52 (2008) 23–37.
[2] J.P.A. Neeft, M. Makkee, J.A. Moulijn, Fuel Process. Technol. 47 (1996) 1–69.
[3] Z. Zhang, D. Han, S. Wei, Y. Zhang, J. Catal. 276 (2010) 16–23.
[4] Q. Shen, G. Lu, C. Du, Y. Guo, Y. Wang, Y. Guo, X. Gong, Chem. Eng. J. 218 (2013) 164–172.
[5] A. Setiabudi, M. Makkee, J.A. Moulijn, Appl. Catal. B Environ. 42 (2003) 35–45.
[6] A. Setiabudi, M. Makkee, J.A. Moulijn, Appl. Catal. B Environ. 50 (2004) 185–194.
[7] G. Busca, Appl. Catal. B Environ. 18 (1998) 1–36.
[8] I. Malpartida, O. Marie, P. Bazin, M. Daturi, X. Jeandel, Appl. Catal. B Environ. 113–114 (2012) 52–60.
[9] E. Aneggi, N.J. Divins, C. de Leitenburg, J. Llorca, A. Trovarelli, J. Catal. 312 (2014) 191–194.
[10] E. Aneggi, C. de Leitenburg, A. Trovarelli, Catal. Today 181 (2012) 108–115.
[11] S. Liu, X. Wu, D. Weng, R. Ran, J. Rare Earths 33 (2015) 567–590.
[12] A. Bueno-López, Appl. Catal. B Environ. 146 (2014) 1–11.
[13] A. Trovarelli, C. de Leitenburg, M. Boaro, G. Dolcetti, Catal. Today 50 (1999) 353–367.
[14] D. Fino, S. Bensaid, M. Piumetti, N. Russo, Appl. Catal. Gen. 509 (2016) 75–96.
[15] S. Fang, L. Wang, Z. Sun, N. Feng, C. Shen, P. Lin, H. Wan, G. Guan, Catal. Commun. 49 (2014) 15–19.
[16] D. Fino, P. Fino, G. Saracco, V. Specchia, Appl. Catal. B Environ. 43 (2003) 243–259.
[17] W.Y. Hernández, M.N. Tsampas, C. Zhao, A. Boreave, F. Bosselet, P. Vernoux, Catal. Today 258 (2015) 525–534.
[18] N. Feng, Y. Wu, J. Meng, C. Chen, L. Wang, H. Wan, G. Guan, RSC Adv. 5 (2015) 91609–91618.
[19] N. Russo, D. Fino, G. Saracco, V. Specchia, J. Catal. 229 (2005) 459–469.
[20] N. Russo, S. Furfori, D. Fino, G. Saracco, V. Specchia, Appl. Catal. B Environ. 83 (2008) 85–95.
[21] A. Mishra, R. Prasad, Clean Technol. Environ. Policy 17 (2015) 2337–2347.
[22] Y. Teraoka, K. Nakano, W. Shangguan, S. Kagawa, Catal. Today 27 (1996) 107–113.
[23] M. Shelef, R. McCabe, Catal. Today 62 (2000) 35–50.
[24] D. Fino, N. Russo, G. Saracco, V. Specchia, J. Catal. 217 (2003) 367–375.
[25] E. Obeid, M.N. Tsampas, S. Jonet, A. Boréave, L. Burel, M.C. Steil, G. Blanchard, K. Pajot, P. Vernoux, Solid State Ion. 262 (2014) 253–256.
[26] E. Obeid, L. Lizarraga, M.N. Tsampas, A. Cordier, A. Boréave, M.C. Steil, G. Blanchard, K. Pajot, P. Vernoux, J. Catal. 309 (2014) 87–96.
[27] A. Serve, T. Epicier, M. Aouine, F.J. Cadete Santos Aires, E. Obeid, M. Tsampas, K. Pajot, P. Vernoux, Appl. Catal. Gen. 504 (2015) 74–80.
[28] R. Baker, J. Guindet, M. Kleitz, J. Electrochem. Soc. 144 (1997) 2427–2432.
[29] F. Liang, W. Zhou, Z. Zhu, ChemElectroChem 1 (2014) 1627–1631.
[30] E. Aneggi, J. Llorca, C. de Leitenburg, G. Dolcetti, A. Trovarelli, Appl. Catal. B Environ. 91 (2009) 489–498.
[31] G. Corro, U. Pal, E. Ayala, E. Vidal, Catal. Today 212 (2013) 63–69.
[32] L. Castoldi, E. Aneggi, R. Matarrese, R. Bonzi, J. Llorca, A. Trovarelli, L. Lietti, Catal. Today 258 (2015) 405–415.
[33] K. Yamazaki, T. Kayama, F. Dong, H. Shinjoh, J. Catal. 282 (2011) 289–298.
[34] K. Yamazaki, Y. Sakakibara, F. Dong, H. Shinjoh, Appl. Catal. Gen. 476 (2014) 113–120.
[35] K. Shimizu, H. Kawachi, S. Komai, K. Yoshida, Y. Sasaki, A. Satsuma, Catal. Today 175 (2011) 93–99.
[36] K. Shimizu, H. Kawachi, A. Satsuma, Appl. Catal. B Environ. 96 (2010) 169–175.
[37] H. Shimokawa, Y. Kurihara, H. Kusaba, H. Einaga, Y. Teraoka, Catal. Today 185 (2012) 99–103.
[38] L. Nossova, G. Caravaggio, M. Couillard, S. Ntais, Appl. Catal. B Environ. 225 (2018) 538–549.
[39] W.Y. Hernández, D. Lopez-Gonzalez, S. Ntais, C. Zhao, A. Boréave, P. Vernoux, Appl. Catal. B Environ. 226 (2018) 202–212.
[40] T.J. Booth, F. Pizzocchero, H. Andersen, T.W. Hansen, J.B. Wagner, J.R. Jinschek, R.E. Dunin-Borkowski, O. Hansen, P. Bøggild, Nano Lett. 11 (2011) 2689–2692.
[41] F. Pizzocchero, M. Vanin, J. Kling, T.W. Hansen, K.W. Jacobsen, P. Bøggild, T.J. Booth, J. Phys. Chem. C 118 (2014) 4296–4302.
[42] K. Mori, K. Watanabe, T. Sato, H. Yamashita, ChemPhysChem 16 (2015) 1347–1351.
[43] D. Gardini, J.M. Christensen, C.D. Damsgaard, A.D. Jensen, J.B. Wagner, Appl. Catal. B Environ. 183 (2016) 28–36.
[44] T. Nanba, S. Masukawa, A. Abe, J. Uchisawa, A. Obuchi, Catal. Sci. Technol. 2 (2012) 1961.
[45] J.P.A. Neeft, O.P. van Pruissen, M. Makkee, J.A. Moulijn, Appl. Catal. B Environ. 12 (1997) 21–31.
[46] J. Zhu, J. Vanommen, A. Knoester, L. Lefferts, J. Catal. 230 (2005) 291–300.
[47] W.-P. Dow, Y.-P. Wang, T.-J. Huang, J. Catal. 160 (1996) 155–170.
[48] S. Liu, X. Wu, W. Liu, W. Chen, R. Ran, M. Li, D. Weng, J. Catal. 337 (2016) 188–198.
[49] M. Skaf, S. Aouad, S. Hany, R. Cousin, E. Abi-Aad, A. Aboukaïs, J. Catal. 320 (2014) 137–146.
[50] Z. Qu, M. Cheng, W. Huang, X. Bao, J. Catal. 229 (2005) 446–458.
[51] X. Zhang, Z. Qu, X. Li, M. Wen, X. Quan, D. Ma, J. Wu, Sep. Purif. Technol. 72 (2010) 395–400.
[52] H. Falsig, B. Hvolbæk, I.S. Kristensen, T. Jiang, T. Bligaard, C.H. Christensen, J.K. Nørskov, Angew. Chem. Int. Ed. 47 (2008) 4835–4839.
[53] C.A. Müller, M. Maciejewski, R.A. Koeppel, R. Tschan, A. Baiker, J. Phys. Chem. 100 (1996) 20006–20014.
[54] D. Martin, D. Duprez, J. Phys. Chem. 100 (1996) 9429–9438.
[55] H.J.M. Bouwmeester, C. Song, J. Zhu, J. Yi, M. van Sint Annaland, B.A. Boukamp, Phys. Chem. Chem. Phys. 11 (2009) 9640.
[56] H. He, H. Dai, C. Au, Catal. Today 90 (2004) 245–254.
[57] S. Ojala, N. Bion, S. Rijo Gomes, R.L. Keiski, D. Duprez, ChemCatChem 2 (2010) 527–533.
[58] V. Ducarme, J.C. Vedrine, J. Chem. Soc. Faraday Trans. 1 Phys. Chem. Condens. Phases 74 (1978) 506.
[59] H. Tsuji, T. Shishido, A. Okamura, Y. Gao, H. Hattori, H. Kita, J. Chem. Soc. Faraday Trans. 90 (1994) 803.
[60] B. Bachiller-Baeza, I. Rodriguez-Ramos, A. Guerrero-Ruiz, Langmuir 14 (1998) 3556–3564.
[61] X.-C. Guo, R.J. Madix, J. Phys. Chem. B 105 (2001) 3878–3885.
[62] G. Corro, S. Cebada, U. Pal, J.L.G. Fierro, J. Catal. 347 (2017) 148–156.
[63] M. Machida, Y. Murata, K. Kishikawa, D. Zhang, K. Ikeue, Chem. Mater. 20 (2008) 4489–4494.
[64] Z. Zhao, V.A.V. Rossi, J.P. Baltrus, P.R. Ohodnicki, M.A. Carpenter, J. Phys. Chem. C 120 (2016) 5020–5032.
[65] M. Haneda, A. Towata, Catal. Today 242 (2015) 351–356.
[66] T. Nanba, S. Masukawa, A. Abe, J. Uchisawa, A. Obuchi, Appl. Catal. B Environ. 123–124 (2012) 351–356.
[67] L.-P. Sun, H. Zhao, Q. Li, L.-H. Huo, J.-P. Viricelle, C. Pijolat, Int. J. Hydrog. Energy 38 (2013) 14060–14066.
[68] B.A.A.L. van Setten, J.M. Schouten, M. Makkee, J.A. Moulijn, Appl. Catal. B Environ. 28 (2000) 253–257.